A Study on the Possibility of Replacing Roller Bearings in CM 120L Concrete Mixers with Necuron 1050 Sliding Bearings

Mirela Romanet
Department of Mechanical Engineering, Doctoral School, Petroleum-Gas University of Ploiesti, Romania
mirelamagic25@yahoo.com

Dragos Gabriel Zisopol
Mechanical Engineering Department, Petroleum-Gas University of Ploiesti, Romania
zisopold@upg-ploiesti.ro (corresponding author)

Mihail Bogdan Roth
Mechanical Engineering Department, Polytechnic University of Bucharest, Romania
rothinimagic@yahoo.com

Dragos Valentin Iacob
Department of Mechanical Engineering, Doctoral School, Petroleum-Gas University of Ploiesti, Romania
dragoshicb@gmail.com

Received: 31 October 2024 | Revised: 20 November 2024 | Accepted: 26 November 2024

 DOI: https://doi.org/10.48084/etasr.9462

ABSTRACT

This paper presents the results of the study on the possibility of replacing the roller bearings of CM 120L concrete mixers with sliding bearings made of Necuron 1050. In order to carry out the study, the radial stresses located in planes normal to the axis of symmetry of a sliding bearing in the cantilever of the material Necuron 1050, were determined using two analytical methods, the finite element method and the electro-resistive tensometry method. An experimental stand was constructed to determine the mechanical and tribological characteristics of the sliding bearings in static and dynamic regimes. The difference between the maximum stress values determined by the two analytical methods is 1.057 MPa, and the difference between the results obtained by Finite Element Analysis (FEA) for static and dynamic stress is 3.093 MPa. The results of the study show that it is recommended to replace a roller bearing with a sliding bearing made of Necuron 1050 polyurethane material.

Keywords-sliding bearings; roller bearings; polyurethane; experimental stand

I. INTRODUCTION

Sliding bearings are essential components in various mechanical applications, providing support and stability for the rotary motion of shafts [1-5]. They are extremely versatile and can be used in a wide range of applications, from industrial equipment to precision machinery [6-11]. The design types of sliding bearings are the following: radial bearings, axial bearings, hydrodynamic bearings, hydrostatic bearings, self-lubricating bearings [12-15]. The material selected for the production of sliding bearings plays an important role in the efficient and durable operation of mechanical equipment and machinery. The main materials used in the manufacture of sliding bearings are: metallic materials (alloyed steels with a high carbon content, stainless steels, bronze, babbitt alloys), non-metallic materials (polyamide, polyurethane, polytetrafluoroethylene), ceramic materials (aluminum oxide, Al 203, silicon carbide), and composite materials (glass or carbon fibers impregnated with resins) [6, 16-19]. The advantages and disadvantages of sliding bearings made of metallic materials and plastic materials are as follows: bearings made of metallic materials are more resistant, their maintenance is cumbersome compared to bearings made of plastic materials, which are better from the technical-economic point of view [19-23].

Polyurethane is a polymer characterized by the repetitive presence of urethane groups [1-3]. Due to its good mechanical properties, this material is used in a wide range of applications in the following fields: automotive, footwear, furniture, construction [4-12]. Studies on Necuron polyurethane material

are limited, which led to this study. Authors in [23] present the influence of defects on the mechanical properties of Necuron. The results of the study show that Necuron 1020 has the highest value of the modulus of elasticity (2790 MPa), at the same time being the stiffest material, and Necuron 1300 is the material that obtained the best results of breaking strength (36.06 MPa). Authors in [24] studied the mechanical behavior in compression and 3-point bending of the specimens made of Necuron 840, Necuron 1020, Necuron 1300, in order to select the optimal material for the production of transtibial prostheses. The conclusions of the study show that Necuron 1300 is the optimal choice for the material used in the manufacture of transtibial prostheses, providing high resistance to compression and bending, as well as optimal elasticity.

This paper presents the study on the possibility of replacing roller bearings of CM 120L concrete mixers with sliding bearings made of Necuron 1050. The replacement of roller bearings with sliding bearings is technically and economically justified by the anti-friction properties of Necuron 1050 and the low price of this material in comparison with the price of bearings.

II. DETERMINATION OF THE RADIAL STRESSES OF SLIDING BEARINGS IN THE CANTILEVER

The CM 120L concrete mixers work with a roller bearing that has a very short service life due to bearing wear under conditions of corrosion and abrasion. In the case of the sliding bearing of the CM 120L concrete mixer, in addition to the radial force, the spindle is subjected to a bending moment that causes it to rotate in the bearing, which causes the axes of the cylinders to become non-parallel, thus changing the contact surfaces. The radial stresses located in planes normal to the axis of symmetry of a sliding bearing in the cantilever of the material Necuron 1050 are determined using two analytical methods.

A. Analytical Methods

The calculation scheme of the sliding bearing is shown in Figure 1 and consists of a simple beam supported at point A and point B, which schematizes the bearing. The loading force F of the concrete mixer is reduced at point C, which is the center of the bearing.

For the numerical calculation of the sliding bearing for CM 120L concrete mixers, we have the following data:

- bearing length L = 80 mm.
- the inner diameter of the bearing d = 28 mm.
- the application force on the bearing F = 1200 N.
- H = 248 mm.

The radial stress is calculated with (1):

$$\sigma_{A,B} = \sigma^N + \sigma^{M_i} = \frac{N}{A} + \frac{M_y}{W_y} \quad (1)$$

and we obtain $\sigma_A = 11{,}036$ MPa and $\sigma_B = 12{,}106$ MPa.

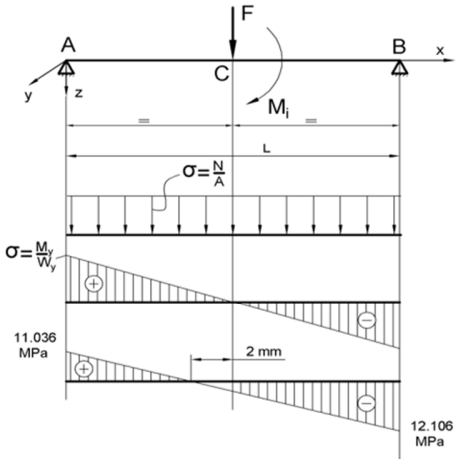

Fig. 1. Bearing calculation scheme – Method 1.

In the method shown in Figure 2, the lateral pressures are assumed to have a triangular variation:

$$M = R \cdot \frac{B}{3} \quad (2)$$

$$M = F\left(H + \frac{B}{2}\right) \quad (3)$$

$$R = \left(\frac{1}{2} \cdot \frac{\pi\, d}{3} \cdot B\right) . p_{max} \quad (4)$$

$$p_{max} = \frac{18\, F\left(H + \frac{B}{2}\right)}{\pi\, B^2 d} \quad (5)$$

Substituting into (5) we obtain $p_{max} = 11.049$ MPa.

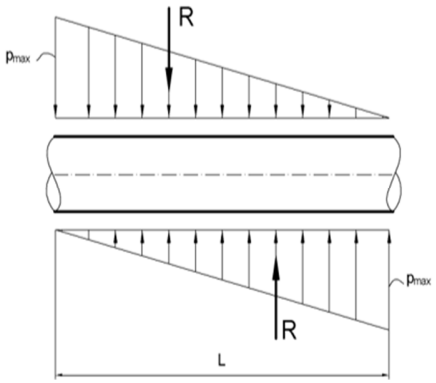

Fig. 2. Bearing calculation scheme – Method 2.

B. Finite Element Analysis

The Finite Element Analysis (FEA) was performed using the ANSYS program [25-26]. The program input data for bearing modeling is shown in Table I for the material Necuron 1050. Table II shows the input data for tree modeling in the ANSYS program. The shaft is made of 25CrMo4 steel. To model the spindle and bushing, the 8-node SOLID 45 element was used, which has 3 degrees of freedom per node: translations in the *x*, *y*, and *z* nodal directions, and to model the contacts between the spindle and the bushing, the pair of elements CONTA 174 – TARG 170 was chosen. In addition, the flexible contact type was selected.

TABLE I. IMPUT DATA FOR BUSH

1	$d = 28$ mm
2	$D = 50$ mm
3	$B = 80$ mm
4	$E_1 = 1250$ MPa
5	$v_1 = 0.42$
6	$\sigma_{comp} = 83$ MPa
7	$j = 0{,}2$ mm (clearance between the bushing and the bearing)

TABLE II. IMPUT DATA FOR SHAFT

1	$d = 28$ mm
2	$H = 248$ mm
3	$F = 1200$ N
4	$E_2 = 2 \cdot 10^5$ MPa
5	$v_2 = 0.3$
6	$\sigma_{comp} = 83$ MPa
7	$j = 0{,}2$ mm (clearance between the bushing and the bearing)

1) *Static Bearing Load*

Figure 3 shows the discretization of the sliding bearing together with the shaft. The bushing consists of 3405 elements.

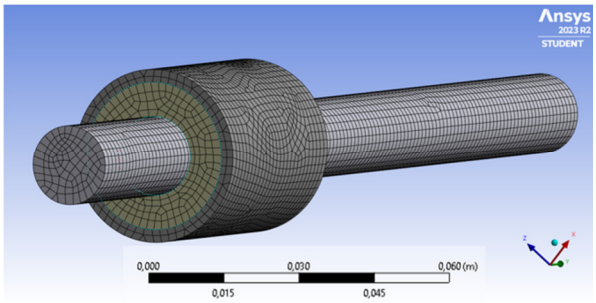

Fig. 3. Discretization of the shaft – bushing adjustment.

Figure 4 shows the stress intensity maps. In particular, Figure 4(a) shows the stress state in the spindle-bush assembly. The bushing is stressed through the spindle to a radial force $F = 1200$ N and a bending moment $M = 345600$ N/mm. Figure 4(b) shows the bushing, and it is observed that the stresses have a semi-cylindrical shape and extend at the ends of the bushing to almost half of it. It can also be seen that the bushing deforms differently. The bushing is compressed in the right half and in the left half.

2) *Dynamic Solicitation of Bearing*

After the bearing is loaded, the shaft begins to rotate clockwise. As the shaft rotates, the tension contour begins to move to the right. Figure 5(a) shows the stress curve in the case where the bushing is subjected to radial force bending and the spindle rotates at a speed of $n = 28$ rpm, there is no clearance between the spindle and the bushing and the friction coefficient is $\mu = 0.3$. The radial stress on the right surface is $\sigma_r = -8.707$ MPa. In Figure 5(b), the bushing is subjected to radial force bending and the spindle rotates at a speed of $n = 28$ rpm, there is a clearance of 0.2 mm between the bushing and the spindle, and the friction coefficient is $\mu = 0.3$. The radial stress on the right surface is $\sigma_r = -11.097$ MPa. It is found that the clearance has an influence on the state of tension in the bearing. Figure 5(c) shows the stress curve for the bushing subjected to bending with radial force and the spindle rotates at a speed of $n = 28$ rpm, there is no clearance between the spindle and the bushing and the friction coefficient is $\mu = 0.6$. The radial stress on the right surface is $\sigma_r = -7.4989$ MPa. In Figure 5(d) the bushing is subjected to radial force bending and the spindle rotates at a speed of $n = 28$ rpm, there is a clearance of 0.2 mm between the bushing and the spindle. The radial stress on the right surface is $\sigma_r = -10.528$ MPa.

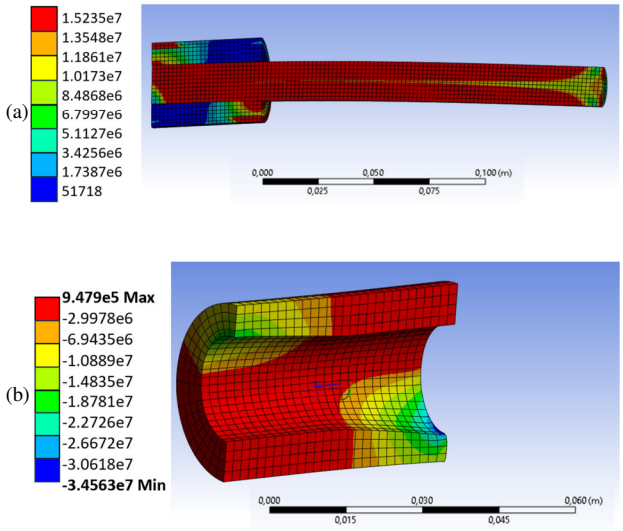

Fig. 4. Stress intensity maps: (a) bushing–shaft assembly, (b) bushing.

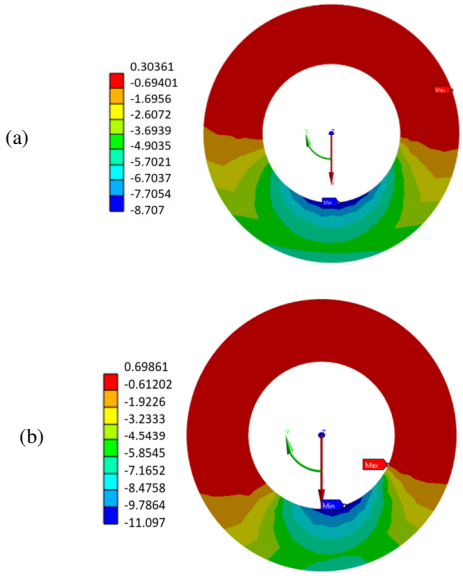

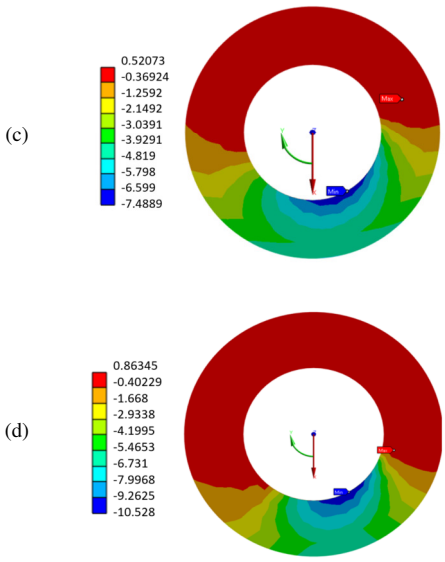

Fig. 5. Modelling of the sliding bearing: (a) without clearance and friction coefficient $\mu = 0.3$; (b) with clearance and friction coefficient $\mu = 0.3$; (c) without clearance and friction coefficient $\mu = 0.6$; (d) with clearance and friction coefficient $\mu = 0.6$.

Table III shows the maximum stresses obtained by the two proposed analytical methods and by the FEA method.

TABLE III. VALUES OF TENSIONS IN THE SLIDING BEARING

Method 1	Method 2	FEA static solicitation	FEA dynamic solicitation
σ_r (MPa)	σ_r (MPa)	σ_{Mises} (MPa)	σ_r (MPa)
-12.106	-11.049	-15	-11.097

The analysis of the centralized data in Table III shows that there is a good agreement between the stresses obtained by all the methods used.

C. Electro-Resistive Tensometry Method

We have designed and built an experimental stand to experimentally determine the stress state at different points in a cantilever sliding bearing. The mechanical and tribological characteristics in static and dynamic mode are determined by the method of resistive tensometry. The experimental stand is the subject of a patent application and is shown in Figure 6. It consists of: 1 – wheels for movement, 2 – frame, 3 – experimental shaft, 4 – Oldham coupling, 5 – engine speed adjustment button, 6 – engine rotation direction change switch, 7 – on/off switch, 8 – electric engine, 9 – speed reducer system with a set of wheels and trapezoidal belts, 10 – digital comparator, 11 – digital dynamometer, 12 – control wheel for adjusting the loading force, and 13 – ring for transferring the force to the force amplifying lever.

1) Static Solicitation Regime

For the static stress regime, the following values were chosen for the magnitude of force F2: 291.36 N; 403.2 N; 481.6 N. Figure 7 shows the variation of the average specific deformations corresponding to the three forces applied to the free end of the shaft for tensometric marks 1 and 2 located on the lower generator.

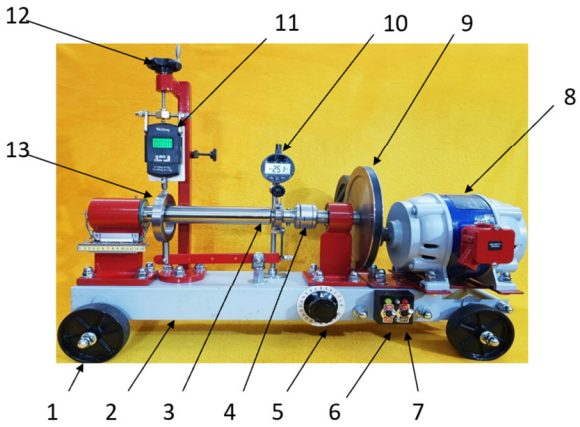

Fig. 6. Experimental stand.

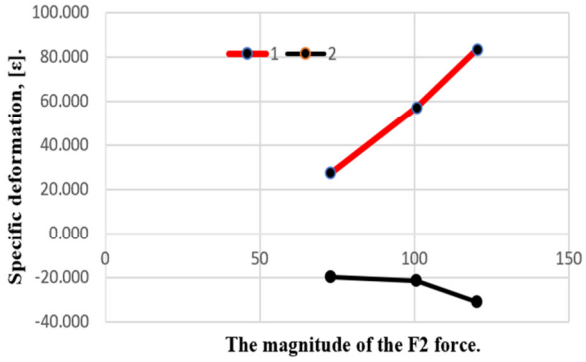

Fig. 7. The variations of the average specific deformations corresponding to the 3 forces applied to the free end of the shaft.

Figures 8 - 10 show the histograms of the deformation variations corresponding to marks 1, located on the lower generator, as well as strain gauge marks 9, 11 located radially at 30 degrees left - right of the vertical axis of the bearing, and the strain gauge marks 10, 12 located radially at 60 degrees left - right of the vertical axis of the bearing, respectively. Each figure corresponds to the force applied to the free end of the bearing.

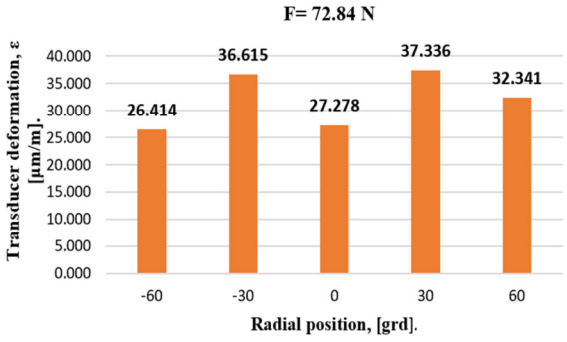

Fig. 8. Strain variations for marks 1, 9, 11, 10, 12, (F = 72.84 N).

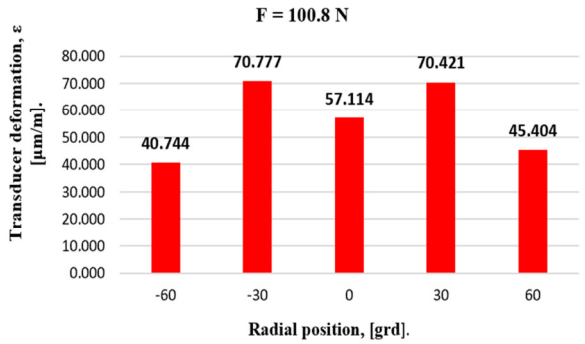

Fig. 9. Strain variations for marks 1, 9, 11, 10, 12, (F = 100.8 N).

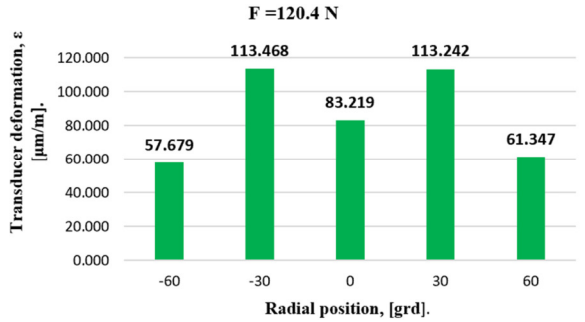

Fig. 10. Strain variations for marks 1, 9, 11, 10, 12, (F = 120.4 N).

2) *Dynamic Solicitation Regime*

For dynamic duty, the motor assembly was a two-stage gear reducer with wheels and V-belts, and the electronic speed control unit was programmed to apply a constant speed of 28 rpm to the cantilever bearing shaft of the stand. Three forces F2: 235.2 N; 306.0 N; 518.8 N were applied with uniform rotation of the cantilever bearing shaft.

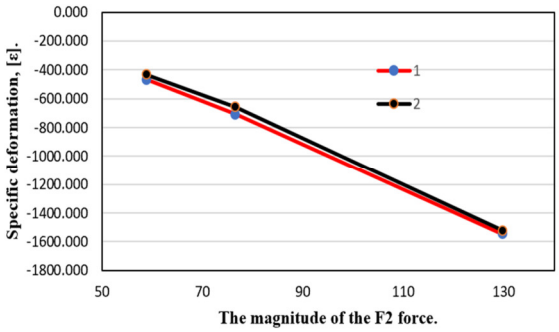

Fig. 11. Variations of the average specific deformations for tensometric marks 1 and 2 corresponding to the 3 forces applied to free end of the shaft.

Figures 12 - 14 show the histograms of the deformation variations corresponding to marks 1, located on the lower generator, as well as strain gauge marks 9, 11 located radially at 30 degrees left - right of the vertical axis of the bearing, and the strain gauge marks 10, 12 located radially at 60 degrees left - right of the vertical axis of the bearing, respectively. Each figure corresponds to the force applied to the free end of the bearing.

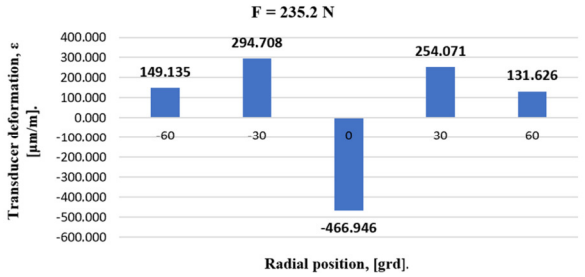

Fig. 12. Strain variations for marks 1, 9, 11, 10, 12, (F = 235.2 N).

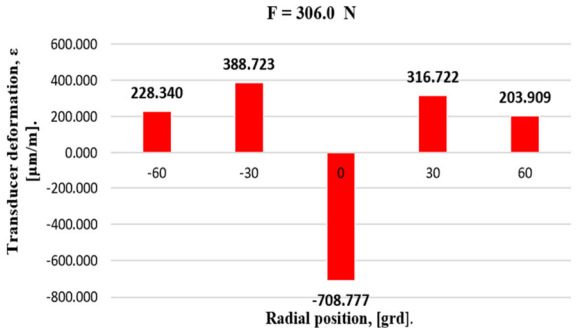

Fig. 13. Strain variations for marks 1, 9, 11, 10, 12, (F = 306 N).

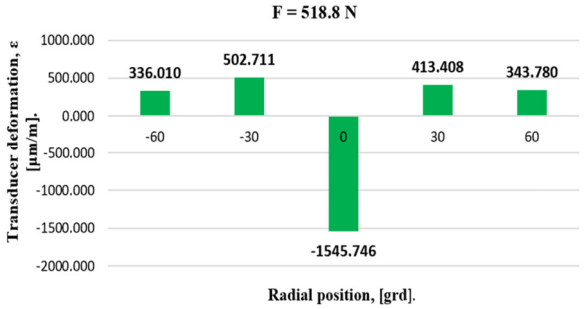

Fig. 14. Strain variations for marks 1, 9, 11, 10, 12, (F = 518.8 N).

As in the case of stress in the static regime, in the dynamic regime the values of the specific deformations of the tensometric marks 1, 9, 11, 10, 12 located radially on the front face of the bearing and symmetrically placed with respect to the vertical plane containing the axis of the bearing, have similar variations. In the dynamic regime, the values of the specific deformations are much higher than in the static regime and the tensometric mark 1 has negative values.

III. CONCLUSIONS

This paper presents the results of the study on the possibility of replacing the roller bearings of the CM 120L concrete mixers with sliding bearings made of Necuron 1050 polyurethane material. The design solution for the stand was the horizontal position, which corresponds to the maximum stress on the bearing for the F2 forces applied to the free end of the shaft. The difference between the maximum stresses obtained by the two analytical methods (see Table III) is 1.057 MPa, (8.73%), and the difference between the results of the Finite Element Analysis (FEA) for static and dynamic stress is 3.093 MPa (26.02%).

The results obtained for the specific deformations of the strain gauges were systematized graphically for both the static and the dynamic regimes with the help of some representations of their variations with the F2 forces applied to the free end of the shaft through graphs and histograms. The values of the specific deformations at all experimentally determined tensometric marks are much higher in the situation of the dynamic stress regime compared to the values obtained in the static stress regime. The variation of the specific deformations of the tensometric marks located on the front face of the bearing are shown in Figures 8 - 10 in the static stress regime, and in Figures 12 - 14 in the dynamic stress regime. The stress state in both variants is relatively small, which proves that the replacement of a roller bearing with a sliding bearing made of Necuron 1050 polyurethane material is recommended. Authors in [24, 25] focused on Necuron 840, Necuron 1001, Necuron 1020, and Necuron 1300. The added value of this study is to broaden the horizon of knowledge regarding the mechanical characteristics of Necuron 1050. At the same time, this study proposes a viable technical-economic solution for the replacement of roller bearings with sliding bearings.

REFERENCES

[1] W. Wang and C. Wang, "Polyurethane for Biomedical Applications: A Review of Recent Developments," in *The Design and Manufacture of Medical Devices*, J. P. Davim, Cambridge, UK: Woodhead Publishing, 2012, ch. 3, pp. 115–151, https://doi.org/10.1533/9781908818188.115.

[2] C. Wang, Z. Xu, Y. Xia, C. Zhang, H. Fang, and K. Sun, "Water Transport Mechanism and Performance Evaluation in Polyurethane Materials: A State-of-the-Art Review," *Polymer Testing*, vol. 138, Sep. 2024, Art. no. 108554, https://doi.org/10.1016/j.polymertesting.2024.108554.

[3] S. P. Zarmehr, M. Kazemi, N. G. A. Madasu, A. J. Lamanna, and E. H. Fini, "Application of Bio-Based Polyurethanes in Construction: A State-of-the-Art Review," *Resources, Conservation and Recycling*, vol. 212, Jan. 2025, Art. no. 107906, https://doi.org/10.1016/j.resconrec.2024.107906.

[4] S. Zafar, R. Kahraman, and R. A. Shakoor, "Recent Developments and Future Prospective of Polyurethane Coatings for Corrosion Protection – A Focused Review," *European Polymer Journal*, vol. 220, Nov. 2024, Art. no. 113421, https://doi.org/10.1016/j.eurpolymj.2024.113421.

[5] J. Lin, J. Liu, J. Shangguan, Z. Fan, D. Wang, and D. Liang, "Application of the Polyurethane Foam Recycling Product as an Asphalt Extender for Sustainable Road Construction," *Construction and Building Materials*, vol. 444, Sep. 2024, Art. no. 137879, https://doi.org/10.1016/j.conbuildmat.2024.137879.

[6] N. Posea, "Săgeți și rotiri la bare încovoiate", în *Rezistența Materialelor*, București, România: Didactică și Pedagogică, 1979, anexa 4, pag.735.

[7] F. B Bowden and D. Tabor, *The Friction and Lubrication of Solids,* Oxford, UK: Oxford University Press, 2001.

[8] B. Bhushan, *Introduction to Tribology*, 2nd ed., Hoboken, New Jersey, USA: Wiley, 2013.

[9] B. Bhushan, *Fundamentals of Tribology and Bridging the Gap Between the Macro- and Micro/Nanoscales*, Dordrecht, Netherlands: Springer, 2001.

[10] B. Bhushan, *Principles and Applications of Tribology*, Hoboken, New Jersey, USA: Wiley, 2013.

[11] S. Cheng, R. Zhang, X. Meng, L. Zheng, and Z. Liu, "Tribological Analysis of Rotor System Startup Considering Deformations of High Elastic Rubber Bushings and Grease Lubricated Plastic Bearings," *Proceedings of the Institution of Mechanical Engineers, Part J: Journal of Engineering Tribology*, Oct. 2024, https://doi.org/10.1177/13506501241292501.

[12] C. N. Chang, J. J. Chung, H. Y. Jiang, and S. J. Ding, "Calcium Silicate Promoting the Upcycling Potential of Polysulfone Medical Waste in Load-Bearing Applications," *Journal of Functional Biomaterials*, vol. 15, no. 11, Oct. 2024, Art. no. 323, https://doi.org/10.3390/jfb15110323.

[13] B. Goerlach, W. Holweger, L. Kitirach, and J. Fliege, "Predicting Wear under Boundary Lubrication: A Decisive Statistical Study," *Lubricants*, vol. 11, no. 12, Dec. 2023, Art. no. 514, https://doi.org/10.3390/lubricants11120514.

[14] L. M. Tichvinsky, "Properties and Performance of Plastic Bearing Materials," *Transactions of the American Society of Mechanical Engineers*, vol. 62, no. 5, pp. 461–465, Feb. 2023, https://doi.org/10.1115/1.4021533.

[15] M. Droß, T. Ossowski, K. Dröder, E. Stockburger, H. Wester, and B. A. Behrens, "Experimental Investigation of Friction-Drilled Bushings for Metal-Plastic In-Mold Assembly," in *Production at the Leading Edge of Technology*, Stuttgart, Germany, 2023, pp. 199–208, https://doi.org/10.1007/978-3-031-18318-8_21.

[16] Z. Jiang, C. Zhang, W. Ni, and S. Li, "A Study on the Temperature Rise Characteristics of High-speed Ball Bearings under Starvation Lubrication," *Industrial Lubrication and Tribology*, vol. 76, no. 10, pp. 1214–1224, Oct. 2024, https://doi.org/10.1108/ILT-06-2024-0208.

[17] C. Pan, Y. Cao, Y. Yan, and R. Shao, "Review of Recent Patents on Smart Bearing," *Recent Patents on Engineering*, vol. 18, no. 4, pp. 13–39, Jun. 2023, https://doi.org/10.2174/1872212118666230427112757.

[18] M. Romanet, I. Nae, R. G. Ripeanu, "Research on tribological behavior of material Necuron 1050," in *15th International Conference on Tribology*, Bucharest, Romania, 2024.

[19] G. Buzdugan and M. Blumenfeld, *Calculul de Rezistență Al Pieselor De Mașini*, București, România: Editura Tehnică, 1979.

[20] V. N. Constantinescu, A. Nica, M. D. Pascovici, G. Ceptureanu, S. Nedelcu, *Lagăre cu alunecare*, București, România: Editura Tehnică, 1980.

[21] N. Dumitru, A. Margine, A. Ungureanu, M. Cherciu, *Organe de Mașini Arbori și Lagăre, Proiectarea prin metode clasice și moderne*, București, România: Editura Tehnică, 2008.

[22] H. L. Dang, "A Study of Single Stone Column Bearing Capacity from a Full-Scale Plate Load Test in Long Son Project," *Engineering, Technology & Applied Science Research*, vol. 14, no. 4, pp. 15602–15606, Aug. 2024, https://doi.org/10.48084/etasr.7698.

[23] M. Jacota, "The Influence of Defects on the Mechanical Properties of Some Polyurethane Materials," *Materiale Plastice*, vol. 50, no. 2, pp. 84–87, Jun. 2013.

[24] J. M. Patrascu and Jacota, "Compression and Bending Tests in order to Evaluate the Use of Necuron for the Manufacturing of Transtibial Prostheses," *Materiale Plastice*, vol. 51, no. 3, pp. 263–266, Sep. 2014.

[25] N. N. Long and N. X. Tung, "Analysis of a Steel-Concrete Composite Plate resting on Axial Bars using the Finite Element Method," *Engineering, Technology & Applied Science Research*, vol. 13, no. 4, pp. 11258–11262, Aug. 2023, https://doi.org/10.48084/etasr.6036.

[26] D. G. Zisopol, D. V. Iacob, and A. I. Portoaca, "A Theoretical-Experimental Study of the Influence of FDM Parameters on PLA Spur Gear Stiffness," *Engineering, Technology & Applied Science Research*, vol. 12, no. 5, pp. 9329–9335, Oct. 2022, https://doi.org/10.48084/etasr.5183.